SCIENCE CHINA
Physics, Mechanics & Astronomy

• Article •

January 2023 Vol. 66 No. 1: 217411
https://doi.org/10.1007/s11433-022-1962-4

Evidence for charge and spin density waves in single crystals of $La_3Ni_2O_7$ and $La_3Ni_2O_6$

Zengjia Liu[1], Hualei Sun[1*], Mengwu Huo[1], Xiaoyan Ma[2,3], Yi Ji[1], Enkui Yi[1], Lisi Li[1], Hui Liu[1], Jia Yu[1], Ziyou Zhang[4], Zhiqiang Chen[4], Feixiang Liang[1], Hongliang Dong[4], Hanjie Guo[5], Dingyong Zhong[1], Bing Shen[1], Shiliang Li[2,3,5], and Meng Wang[1*]

[1] *Center for Neutron Science and Technology, Guangdong Provincial Key Laboratory of Magnetoelectric Physics and Devices, School of Physics, Sun Yat-sen University, Guangzhou 510275, China;*
[2] *Beijing National Laboratory for Condensed Matter Physics, Institute of Physics, Chinese Academy of Sciences, Beijing 100190, China;*
[3] *School of Physical Sciences, University of Chinese Academy of Sciences, Beijing 100049, China;*
[4] *Center for High Pressure Science and Technology Advanced Research, Shanghai 201203, China;*
[5] *Songshan Lake Materials Laboratory, Dongguan 523808, China*

Received June 14, 2022; accepted July 13, 2022; published online November 1, 2022

Charge and spin orders are intimately related to superconductivity in copper oxide superconductors. Elucidation of the competing orders in various nickel oxide compounds is crucial, given the fact that superconductivity has been discovered in $Nd_{0.8}Sr_{0.2}NiO_2$ films. Herein, we report structural, electronic transport, magnetic, and thermodynamic characterizations of single crystals of $La_3Ni_2O_7$ and $La_3Ni_2O_6$. $La_3Ni_2O_7$ is metallic with mixed Ni^{2+} and Ni^{3+} valent states. Resistivity measurements yield two transition-like kinks at ~110 and 153 K. The kink at 153 K is further revealed from magnetization and specific heat measurements, indicative of the formation of charge and spin density waves. $La_3Ni_2O_6$ single crystals obtained from the topochemical reduction of $La_3Ni_2O_7$ are insulating and show an anomaly at ~176 K on magnetic susceptibility. The transition-like behaviors of $La_3Ni_2O_7$ and $La_3Ni_2O_6$ are analogous to those observed in $La_4Ni_3O_{10}$ and $La_4Ni_3O_8$, suggesting that charge and spin density waves are a common feature in the ternary La-Ni-O system with mixed-valent states of nickel.

charge-density-wave systems, spin-density waves, mixed-valence solids, superlattices, crystal growth

PACS number(s): 71.45.Lr, 75.30.Fv, 75.30.Mb, 75.70.Cn, 81.10.Fq

Citation: Z. Liu, H. Sun, M. Huo, X. Ma, Y. Ji, E. Yi, L. Li, H. Liu, J. Yu, Z. Zhang, Z. Chen, F. Liang, H. Dong, H. Guo, D. Zhong, B. Shen, S. Li, and M. Wang, Evidence for charge and spin density waves in single crystals of $La_3Ni_2O_7$ and $La_3Ni_2O_6$, Sci. China-Phys. Mech. Astron. **66**, 217411 (2023), https://doi.org/10.1007/s11433-022-1962-4

1 Introduction

The recent discovery of superconductivity in $Nd_{0.8}Sr_{0.2}NiO_2$ films has aroused great research enthusiasm in the search for superconductivity and understanding of the pairing mechanism in nickel oxide system [1-3]. In particular, whether or not the mechanisms of the superconductivity in nickelates and copper oxide superconductors are the same remains an open question. The superconductivity, spin order, and charge order could be tuned by carrier doping in cuprates, and it is widely accepted that the static and dynamic spin and charge orders play a crucial role in the mechanism of superconduc-

*Corresponding authors (Hualei Sun, email: sunhlei@mail.sysu.edu.cn; Meng Wang, email: wangmeng5@mail.sysu.edu.cn)

© Science China Press and Springer-Verlag GmbH Germany, part of Springer Nature 2022

tivity [4,5].

The ternary nickel oxide *Ln*-Ni-O system (*Ln* = La, Pr, Nd, Sm, and Eu) contains the Ruddlesden-Popper (RP) compounds $Ln_{n+1}Ni_nO_{3n+1}$, which possess *n* layers of perovskite-type $LnNiO_3$, separated by a single rocksalt *Ln*O layer along the *c* axis [6-10]. The Ni ions exhibit mixed valences of Ni^{3+} ($3d^7$) and Ni^{2+} ($3d^8$) (Table 1). By a topochemical reduction method, two apical oxygen atoms of a NiO_6 octahedron could be removed, causing the remaining oxygen atoms to rearrange and result in a fluorite *Ln*-O_2-*Ln* layer, as is shown in Figure 1. The topochemical reduced compounds $Ln_{n+1}Ni_nO_{2n+2}$ consist of the mixed-valent states of Ni^{1+} ($3d^9$) and Ni^{2+} (Table 1). The structures of the RP system and the RP reduced system are analogous to the ternary *Ln*-Cu-O system, especially the Ni-O planes that are regarded as alternative superconducting planes similar to the Cu-O planes in cuprates. Theorists suggested that superconductivity may be induced by doping low-spin Ni^{2+} ($S = 0$) to a nickelate antiferromagnetic (AF) insulator with Ni^{1+} ($S = 1/2$) in square planar coordination with O ions [11,12]. This could be realized in the chemical reduced RP phase $Ln_{n+1}Ni_nO_{2n+2}$ by hole doping on the *Ln* site, such as Sr doped $Ln_{0.8}Sr_{0.2}NiO_2$,

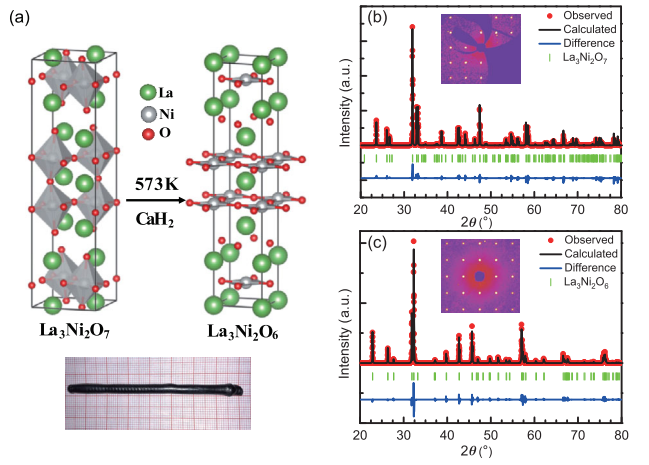

Figure 1 (Color online) (a) Sketches of the crystal structures of $La_3Ni_2O_7$ and $La_3Ni_2O_6$. A photo of a single crystal of $La_3Ni_2O_7$. (b) X-ray diffraction patterns integrated from single crystal diffraction on $La_3Ni_2O_7$ and (c) $La_3Ni_2O_6$. The insets in (b) and (c) are diffraction patterns in reciprocal space on the corresponding single crystals collected on a single crystal X-ray diffractometer.

Table 1 Empirical formula, corresponding *n*, and the average Ni valence of the RP phases $Ln_{n+1}Ni_nO_{3n+1}$ and the topochemical reduced phases $Ln_{n+1}Ni_nO_{2n+2}$, *Ln* = La, Pr, Nd, Sm, and Eu

n	$Ln_{n+1}Ni_nO_{3n+1}$		$Ln_{n+1}Ni_nO_{2n+2}$	
	Composition	Ni valence	Composition	Ni valence
∞	113	+3	112	+1
3	4310	+2.67	438	+1.33
2	327	+2.5	326	+1.5
1	214	+2	–	–

where *Ln*=La, Nd, and Sm. Superconductivity has been indeed observed in films of these hole doped compounds and $Nd_6Ni_5O_{12}$, where nickel ions exhibit an average valence of +1.2 [13-15]. The transition temperature T_c of the superconducting films could be enhanced by pressure [16]. However, superconductivity has not been observed in bulk samples of the *Ln*-Ni-O system under ambient or high pressure [8,17-19].

Progress on studies of charge and spin orders has been made because of the availability of high quality single crystals for the La-Ni-O system grown by the floating zone technique with high oxygen pressure [20,21]. Antiferromagnetic transitions were identified on metallic $LaNiO_3$ ($n = \infty$) and $La_4Ni_3O_{10}$ ($n = 3$) single crystals by neutron scattering studies, which were absent for previous measurements on powder samples [22-24]. The AF transition has been ascribed to the spin density wave (SDW) that originates from Fermi surface nesting, differing from the spin order in doped $n = 1$ $La_{2-x}Sr_xNiO_4$ and cuprates. A charge density wave (CDW) coincident with the SDW was found in $La_4Ni_3O_{10}$ and was suggested to result in a metal-to-metal transition [23]. For the topochemically reduced product $La_4Ni_3O_8$, synchrotron X-ray and neutron diffraction also reveal stacked charge and spin stripes weakly correlated along the *c* axis [25,26]. In this case, $La_4Ni_3O_8$ is an insulator and the charge and spin orders result from the competition among Coulomb repulsion, spin orbital coupling, and magnetic exchange interaction.

The $n = 2$ RP compound $La_3Ni_2O_7$ and chemical reduced product $La_3Ni_2O_6$ consisting of the bilayer NiO_2 planes are analogous to the trilayer $La_4Ni_3O_{10}$ and $La_4Ni_3O_8$ in structural and physical properties [27-33]. Theoretical calculations for $La_3Ni_2O_7$ and $La_4Ni_3O_{10}$ suggest the existence of a hidden one-dimensional Fermi surface nesting that would result in CDW instability [34,35]. For $La_3Ni_2O_6$ and $La_4Ni_3O_8$, charge-ordered related structural distortion and magnetic order will emerge in the ground state [36]. The electronic density of states of $La_3Ni_2O_7$ indeed has an abrupt change at around 100-120 K, reflected in both the Hall coefficient and the Seebeck coefficient [27,29,30]. However, neutron diffraction [31], resistivity, and magnetic susceptibility measurements on powder samples of $La_3Ni_2O_7$ that were synthesized through the soft chemistry method did not reveal evidence of a charge or spin density wave [27-31]. $La_3Ni_2O_6$ has raised great interest because of the similarities of the electronic structures to cuprates and the possible realization of superconductivity through tuning the valence by carrier doping or high pressure [12,37]. Moreover, nuclear magnetic resonance (NMR) studies on $La_3Ni_2O_6$ powder samples suggest the existence of magnetic interactions; however, the basic magnetic properties remain unclear [38]. In fact, a comprehensive study of $La_3Ni_2O_7$ and $La_3Ni_2O_6$

is lacking because of the unavailability of single crystals. Single crystal growth of samples with the average valences of nickel ions larger than +2 requires high pressure oxygen, and the pressure window is narrow for a specific compound [21]. However, single crystals are crucial for investigations of the possible emerging density waves of charge and spin in $La_3Ni_2O_7$ and $La_3Ni_2O_6$ in order to ascertain the universality of the ternary nickel oxide system and pave the way for further manipulation of the states of nickel, with the possible realization of superconductivity [37].

Here, we report the successful growth of $La_3Ni_2O_7$ single crystals via the high oxygen pressure floating zone technique and the achievement of $La_3Ni_2O_6$ single crystals through a subsequent low temperature topochemical reduction method [21]. Electrical resistivity measurements on single crystals of $La_3Ni_2O_7$ and $La_3Ni_2O_6$ showed distinct properties. $La_3Ni_2O_7$ is metallic, whereas $La_3Ni_2O_6$ is insulating. Superconductivity was not realized in $La_3Ni_2O_6$ under pressures up to 25.3 GPa. Anomalies in resistivity, susceptibility, and specific heat that may correspond to spin and charge waves were observed in both compounds. The results indicate the emergent orders of charge and spin are universal for the nickelates with mixed-valent states of nickel.

2 Experimental methods

Polycrystalline samples were synthesized through the standard solid-state reaction techniques. Stoichiometric amounts of La_2O_3 and an excess of 0.5% NiO (Macklin, 99.99%) were thoroughly ground. The excess of 0.5% NiO was used to compensate for the loss of volatilization. The ground mixtures were made into pellets and then sintered at 1100°C for 50 h. After cooling down to room temperature, the reactants were reground and then formed into pellets for sintering again. The procedures were repeated three times to ensure a complete and homogeneous reaction [21]. The seed and feed rods were prepared by pressurizing the powders under hydrostatic pressure and then sintering at 1400°C for 12 h. The rods were approximate 9 cm in length and 0.6 cm in diameter.

High oxygen pressure is crucial for the synthesis of the homologous RP system of nickelates. A vertical optical-image floating zone furnace designed for a 100 bar high pressure (HKZ, SciDre, Dresden) was employed in our single crystal growth. $La_3Ni_2O_7$ single crystals were grown with an oxygen pressure at $p(O_2)$=15 bar and a 5 kW Xenon arc lamp. The traveling rate was 3 mm/h after a fast traveling procedure at 10 mm/h to improve the density. Afterward, the feed and seed rods counter-rotate at 15 and 10 r/min, respectively, in order to improve the homogeneity. $La_3Ni_2O_6$ was obtained from the $La_3Ni_2O_7$ single crystals by a topochemical reduction method. $La_3Ni_2O_7$ single crystals were enclosed in aluminum foil and then sealed in a vacuum with stoichiometric CaH_2 powders. The reaction proceeded under the condition of 300°C for four days.

X-ray photoemission spectroscopy (XPS) measurements were carried out on an XPS machine (Escalab 250 Xi, Thermo Fisher). Argon sputtering was adopted to remove the surface contamination. The sputtering depth was about 100 nm. The monochromatic Al Kα radiation with a photon energy of 1486.6 eV was applied to analyze the valent states of nickel. The X-ray beam was focused on a 0.5 mm spot surface. In order to obtain high-resolution spectra, the electron energy analyzer was operated at a pass energy of 30 eV. The C 1 s photoelectron line (284.8 eV) was used to calibrate the binding energies of the photoelectrons.

Magnetic susceptibility, resistivity, and specific heat measurements were performed on a physical property measurement system (quantum design). *In situ* high pressure electrical resistance measurements were carried out in a diamond anvil cell made from a Be-Cu alloy using a standard four-probe technique [39, 40]. NaCl powders were employed as the pressure transmitting medium. The pressure in the resistance measurements was calibrated by the ruby fluorescence shift at room temperature. Single crystal X-ray diffraction (XRD) was performed on a single crystal X-ray diffractometer (SuperNova, Rigaku) with Mo-Kα radiation at 300 K. The crystal structure was solved with the direct method and refined using the full-matrix least-squares method [41]. Energy-dispersive X-ray spectroscopy (EDS) (EVO, Zeiss) was employed to determine the compositions of the crystals. In addition, the Laue XRD technique was utilized to confirm the crystal orientation and level of crystallinity.

3 Results

3.1 $La_3Ni_2O_7$

Crystal structures of $La_3Ni_2O_7$ and $La_3Ni_2O_6$ are shown in Figure 1(a). $La_3Ni_2O_7$ crystallizes in orthorhombic symmetry (space group: *Cmcm*) with distorted vertex-sharing NiO_6 octahedra and rocksalt La-O layers [31]. The structure can be termed as an inter-growth of two NiO_6 octahedra planes and a La-O fluorite-type layer, stacking along the *c* direction. $La_3Ni_2O_6$ with the apical oxygen atoms removed crystallizes in tetragonal symmetry (space group: *I*4/*mmm*). The structure is stacked by two corner-sharing square NiO_2 planes and a La-O fluorite-type layer along the *c* direction [42]. The XRD patterns measured on single crystals reveal the high quality of our samples (Figure 1(b) and (c)). Detailed structural parameters are summarized in Table 2.

The compositions of the single crystals determined by EDS are $La_{2.95}Ni_2O_7$ and $La_{2.92}Ni_2O_6$ close to the stoichiometric compositions within the instrumental accuracy. We note the oxygen content is not determined in EDS, and the contents of La have been normalized by those of Ni.

The valent states of Ni are crucial for the realization of charge and spin density waves. $La_3Ni_2O_7$ is metallic, where nickel ions could host a valence of +2.5 or mixed-valent states of +2 and +3. Figure 2(a) shows the XPS spectrum of Ni ions in $La_3Ni_2O_7$. For comparison, an XPS spectrum of Ni^{2+} measured on NiO is presented in Figure 2(b). The main peaks of the spectrum of Ni^{2+} are located at 853.6 and 855.6 eV. In addition, a broad satellite peak appears at a higher binding energy of 860.8 eV. These features are typical for nickel ions with a divalent oxidation state. The XPS spectrum of $La_3Ni_2O_7$ exhibits asymmetric doublet peaks at 853.0 and 855.7 eV, as is shown in Figure 2(a). We preserve the ratio of the two peaks of Ni^{2+} measured on NiO and fit the spectrum of $La_3Ni_2O_7$. The peak at 855.7 eV could be separated, yielding the existence of the trivalent oxidation state [43-45]. Thus, our XPS measurements reveal that the valent states of nickel in $La_3Ni_2O_7$ are a mixture of the divalent Ni^{2+} and trivalent Ni^{3+} oxidation states.

Table 2 Structural parameters for single crystals of $La_3Ni_2O_7$ and $La_3Ni_2O_6$ at 300 K measured with Mo-Kα radiation with λ = 0.7107 Å. The data were collected in the range of $1.171° \le 2\theta \le 40.84°$

Empirical formula	$La_3Ni_2O_7$	$La_3Ni_2O_6$
Space group	*Cmcm* (Orthorhombic)	*I*4/*mmm* (Tetragonal)
Unit-cell parameters	a = 5.4000(7) Å b = 5.4384(7) Å c = 20.455(4) Å $\alpha = \beta = \gamma = 90°$	$a = b$ = 3.9720(4) Å c = 19.368(4) Å $\alpha = \beta = \gamma = 90°$
La1	(0.32, 0.75, 0.25)	(1, 1, 0.5)
La2	(0.5, 0.25, 0.75)	(1, 0, 0.32)
Ni	(0.40, 0.75, 0.75)	(0.5, 0.5, 0.42)
O1	(0.41, 1, 1)	(1, 0.5, 0.42)
O2	(0.5, 0.71, 0.75)	(0.5, 0, 0.25)
O3	(0.40, 0.5, 0.5)	–
O4	(0.30, 0.78, 0.75)	–
Goodness-of-fit on F^2	1.184	0.966
Final R indexes (all data)	R_1=0.0327	R_1=0.0469

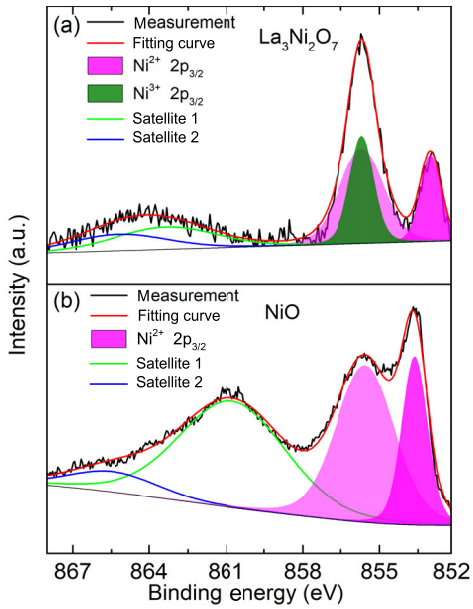

Figure 2 (Color online) XPS measurements of the Ni 2p core levels for (a) $La_3Ni_2O_7$ and (b) NiO. The pink areas and satellites 1 and 2 in (b) are deconvoluted of the Ni $2p_{3/2}$ XPS data. The ratio of the two main peaks for Ni^{2+} is preserved in the fitting of the Ni 2p core levels for $La_3Ni_2O_7$ in (a). The black solid lines are the experimental data. The red line is a fit of the total intensities.

Figure 3(a) shows the temperature dependence of the resistance for $La_3Ni_2O_7$ single crystals, revealing a metallic ground state that is analogous to the n = 3, and ∞ RP compounds [22, 28, 46, 47]. We observe two anomalies in resistance: one at ~110 K and the other at 153 K. These anomalies could be identified unambiguously in the deviation of resistance against temperature dR/dT, as is shown in Figure 3(a). The former one at ~110 K is close to the anomalies observed in the Hall and Seebeck coefficients [27, 29, 30]. The latter one at 153 K is weaker and has not been identified in the previous measurements on powder samples. For $LaNiO_3$ and $La_4Ni_3O_{10}$, a metal-metal transition near 150 K has been observed in resistivity, where the origin has been proved to result from intertwined charge and spin density waves [22, 23].

To investigate the origin of the transitions in $La_3Ni_2O_7$, we

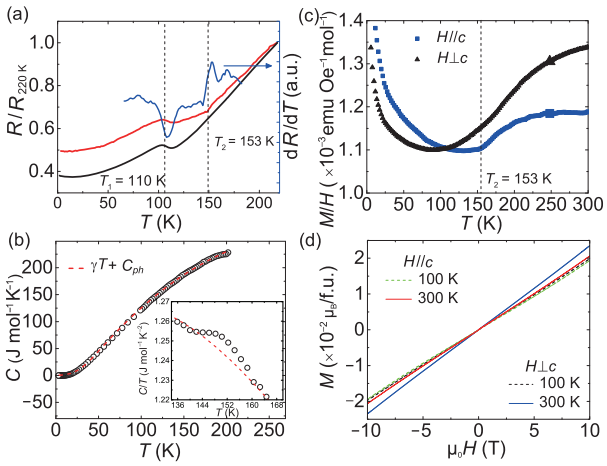

Figure 3 (Color online) (a) The red and black lines denote the resistance of two $La_3Ni_2O_7$ single crystals as a function of temperature. The blue line is the derivative of the resistance in red. (b) Temperature dependence of the total specific heat of $La_3Ni_2O_7$. The dashed line is the fit of the formula described in the text. The inset shows an abnormal change at ~153 K. (c) Magnetization of $La_3Ni_2O_7$ measured at a magnetic field of μ_0H = 0.4 T parallel to and perpendicular with the c axis under zero-field cooled condition. (d) Magnetization against the magnetic field μ_0H for $H//c$ and $H\perp c$ at 100 and 300 K.

measured the specific heat and magnetization against temperature and magnetic field. The specific heat for temperatures between 3 and 200 K is shown in Figure 3(b). A model $C=\gamma T + C_{ph}$ was employed to fit the data, where γT and C_{ph} represent the contributions of electrons and phonons, respectively. A modified Debye model considering the existence of two phonon modes that reconcile the heavy atoms (La and Ni) and light atoms (O) was considered to describe the phonon contribution, $C_{ph} = 9R\sum_{n=1}^{2} C_n\left(\frac{T}{\theta_{Dn}}\right)^3 \int_0^{\theta_{Dn}/T} \frac{x^4 e^x}{(e^x-1)^2} dx$, where R=8.314 J mol^{-1} K^{-1} is the ideal gas constant, and C_n represents the numbers of the heavy or light atoms in a formula unit. The modeling reveals that, of the 12 atoms in the formula unit, 5 atoms have a Debye temperature θ_{D1} of (298 ± 3) K and 7 atoms have a Debye temperature θ_{D2} of (620 ± 4) K [48, 49]. The fitting also yields γ=7.3 mJ mol^{-1} K^{-2}, close to the value of 6.4 mJ mol^{-1} K^{-2} revealed from powder samples [34]. With the estimated densities of charge-carriers and the mass of the free-electrons, the value of the electron effective mass m^*/m_0 of $La_3Ni_2O_7$ is ≈ 2.12, similar to 2.56 for $La_4Ni_3O_{10}$ and much lower than 15 for $LaNiO_3$ [27, 32, 50]. The effective mass of electrons suggests that the electronic correlations in $La_3Ni_2O_7$ and $La_4Ni_3O_{10}$ are weaker than that of the n=∞ compound $LaNiO_3$. The anomaly at 153 K could also be observed in specific heat, as is shown in the inset of Figure 3(b), consistent with the temperature of the anomaly at 153 K in resistance.

Figure 3(c) displays the temperature dependence of the magnetization of $La_3Ni_2O_7$ single crystals at 4000 Oe. The kink at ~153 K for $H//c$ could be identified in magnetization, suggesting the same physical origin as that of the anomalies at the identical temperature in resistance and specific heat. In contrast, the anomaly at ~110 K in resistance does not appear in magnetization. The upturn below 50 K with decreasing temperature in Figure 3(c) may be related to magnetic impurities or lattice imperfections. We note the magnetization of $La_3Ni_2O_7$ single crystals shown in Figure 3(c) is reminiscent of that observed in $LaNiO_3$ and $La_4Ni_3O_{10}$ single crystals [22, 23]. For the two materials, an intertwined charge and SDW has been confirmed by neutron and XRD measurements. The magnetization as a function of magnetic field and temperature is shown in Figure 3(d). The magnetization increases linearly against the magnetic field up to $\mu_0 H$ = 10 T, indicating antiferromagnetic correlations.

3.2 $La_3Ni_2O_6$

The ground state of $La_3Ni_2O_6$ with mixed $Ni^{1+}d^9$ (S = 1/2) and $Ni^{2+}d^8$ (S = 0) was predicted to be an AF insulator with a checkerboard charge order and both AF and ferromagnetic (FM) interactions. Pressure will suppress the FM interactions further and may induce superconductivity [36]. However, only the insulating state was confirmed due to the limitation of powder samples [37]. We obtained single crystals of $La_3Ni_2O_6$ from the topochemical reduction of the $La_3Ni_2O_7$ single crystals. Temperature dependence of the electrical resistivity ρ is shown in Figure 4(a) and the inset. The semiconducting behavior is analogous to the measurements on powder samples [37]. The resistivity of $La_3Ni_2O_6$ displays a weak kink at 101 K, in contrast to the abrupt change in resistivity at ~100 K for $La_4Ni_3O_8$ that corresponds to the formation of charge and spin stripe orders [25, 26]. By fitting the resistivity to the activation energy model $\rho(T) = \rho_0 \exp(E_a/k_B T)$, two thermal activation energy gaps of E_a = 54 and 100 meV are obtained, corresponding to 84 ≤ T ≤ 125 K and 176 ≤ T ≤ 300 K, respectively. To explore the possible superconductivity in $La_3Ni_2O_6$, the resistance was measured under pressure up to 25.3 GPa, as is shown in Figure 4(b). The metallization is achieved at 6.1 GPa. However, no superconductivity emerges in the pressure range we measured. The small upturn in resistance at low temperature under pressure may result from magnetic impurity or oxygen deficiency.

Figure 4(c) displays the magnetization of $La_3Ni_2O_6$ with the magnetic field perpendicular to the c axis. A kink at ~176 K could be identified in the derivative of the magnetization for the magnetic fields at 1 and 2 T. As theory suggests, the kink in magnetization at 176 K may be associated with the charge and spin orders of $La_3Ni_2O_6$ [36], which may also result in the change of the fitted thermal activation

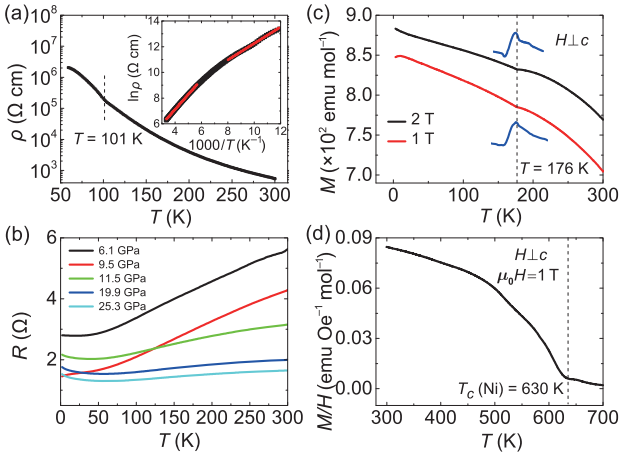

Figure 4 (Color online) (a) Resistivity of $La_3Ni_2O_6$ measured as a function of temperature. The dashed line indicates a weak kink at 101 K. The inset shows a fit with $\rho(T) = \rho_0 \exp(E_a/k_B T)$, resulting in E_a = 54 meV for 84 ≤ T ≤ 125 K and E_a = 100 meV for 176 ≤ T ≤ 300 K. (b) Resistance at various pressures applied with a diamond anvil cell. (c) Magnetization measured with magnetic fields of $\mu_0 H$ = 1 and 2 T and perpendicular to the c axis. The blue lines show derivatives of the magnetization. The dashed line indicates a kink at 176 K. (d) High-temperature magnetization measured with $\mu_0 H$ = 1 T and $H \perp c$. The dashed line indicates the ferromagnetic transition of Ni at 630 K.

gaps against temperature, as is shown in the inset of Figure 4(a). The magnetization decreases as the temperature increases, similar to the behavior of a ferromagnet. It is known that the topochemical reduction method induces Ni impurities [18]. A high-temperature magnetization measurement was conducted, revealing a FM transition at T_c = 630 K, as is shown in Figure 4(d). The result demonstrates the existence of Ni impurities. The quality of the $La_3Ni_2O_6$ single crystals obtained from the topochemical reduction of $La_3Ni_2O_7$ is poor. We failed to observe the kink at 101 or 176 K in specific heat. Further investigations of neutron and XRD on higher quality single crystals are required.

4 Discussion and summary

The mixed-valent and spin states of Ni in the ternary La-Ni-O system tend to form charge and spin orders. The emergence of the two types of order has been verified in hole doped $La_{2-x}Sr_xNiO_4$ (x =1/4, 1/3, and 1/2), $La_4Ni_3O_{10}$, and $La_4Ni_3O_8$ [25,26,51-53]. For the trilayer RP compounds, the ratio of the magnetic Ni^{3+} (S = 1/2) and nonmagnetic Ni^{2+} (S = 0) is 2:1; for the bilayer RP compounds, the value of this ratio drops to 1:1. The formation of CDW is expected, whereas the SDW may be weaker in the bilayer compounds. The changes in resistivity, susceptibility, and specific heat at 153 K are indeed less pronounced in $La_3Ni_2O_7$ single crystals compared to those of $La_4Ni_3O_{10}$. The possibility of the CDW emerging in the bilayer La-Ni-O system unaccompanied by the SDW could not be ruled out. In this case, the anomaly in magnetization could be due to charge-spin interactions. Our Raman scattering measurements on $La_3Ni_2O_7$ also revealed an anomaly at ~150 K for the position of the peak at ~597 cm^{-1} (data not shown). Based on previous studies, the anomaly in resistance at ~110 K may be related to the change of carrier concentration induced by a structural evolution against temperature [27-31].

For $La_3Ni_2O_6$, an insulating ground state with a checkerboard charge order and AF order based on Ni^{1+} is expected [36]. The observed kinks in resistivity and magnetization may be related to the charge and spin orders. The average valence of Ni, +1.5, is close to +1.2 of the superconducting film samples. However, superconductivity does not appear up to 25.3 GPa, where the samples exhibit metallic character [37]. The superconductivity seems to be sensitive to the average-valent state of nickel. In addition, the possible charge and spin orders in $La_3Ni_2O_6$ may suppress superconductivity under pressure. Further synchrotron X-ray and neutron diffraction studies on single crystal samples of the bilayer compounds are necessary to demonstrate the charge and spin orders.

In summary, we grew bilayer nickelate $La_3Ni_2O_7$ and $La_3Ni_2O_6$ single crystals successfully via the floating zone method with high pressure of oxygen. The structural, magnetic, electronic, and specific heat properties of both compounds were characterized in detail. Electronic measurements showed metallic character for $La_3Ni_2O_7$ and semiconducting character with a thermal activation gap of 55 meV for $La_3Ni_2O_6$. The resistance, magnetization, and specific heat all reveal a transition-like anomaly at 153 K for $La_3Ni_2O_7$, suggesting the formation of CDW and SDW. In addition, the magnetization of $La_3Ni_2O_6$ also yields a kink at 176 K, reminiscent of the charge and spin density waves in $La_3Ni_2O_7$. Pressures above 6.1 GPa could metallize $La_3Ni_2O_6$. However, no superconductivity was observed up to 25.3 GPa. Our data suggest the formation of charge and spin density waves in metallic compounds and orders in semiconducting and insulating compounds may be a universal characteristic for nickelates with mixed-valent states of nickel.

This work was supported by the National Natural Science Foundation of China (Grant Nos. 12174454, 11904414, 11904416, and U2130101), the Guangdong Basic and Applied Basic Research Foundation (Grant No. 2021B1515120015), the Guangzhou Basic and Applied Basic Research Foundation (Grant No. 202201011123), and the National Key Research and Development Program of China (Grant Nos. 2019YFA0705702, 2020YFA0406003, 2021YFA1400401, and 2021YFA0718900).

1 D. Li, K. Lee, B. Y. Wang, M. Osada, S. Crossley, H. R. Lee, Y. Cui, Y. Hikita, and H. Y. Hwang, Nature **572**, 624 (2019).
2 Q. Gu, and H. H. Wen, Innovation **3**, 100202 (2022), arXiv: 2109.07654.
3 Q. Gao, Y. Zhao, X. J. Zhou, and Z. Zhu, Chin. Phys. Lett. **38**, 077401 (2021), arXiv: 2102.10292.
4 B. Vignolle, S. M. Hayden, D. F. McMorrow, H. M. Rønnow, B. Lake, C. D. Frost, and T. G. Perring, Nat. Phys. **3**, 163 (2007).
5 B. Keimer, S. A. Kivelson, M. R. Norman, S. Uchida, and J. Zaanen, Nature **518**, 179 (2015).
6 G. M. Zhang, Y. Yang, and F. C. Zhang, Phys. Rev. B **101**, 020501 (2020), arXiv: 1909.11845.
7 Y. Zhang, L. F. Lin, W. Hu, A. Moreo, S. Dong, and E. Dagotto, Phys. Rev. B **102**, 195117 (2020), arXiv: 2008.04392.
8 B. X. Wang, H. Zheng, E. Krivyakina, O. Chmaissem, P. P. Lopes, J. W. Lynn, L. C. Gallington, Y. Ren, S. Rosenkranz, J. F. Mitchell, and D. Phelan, Phys. Rev. Mater. **4**, 084409 (2020), arXiv: 2006.09548.
9 K. W. Lee, and W. E. Pickett, Phys. Rev. B **70**, 165109 (2004), arXiv: cond-mat/0405570.
10 Q. Li, C. P. He, X. Y. Zhu, J. Si, X. W. Fan, and H. H. Wen, Sci. China-Phys. Mech. Astron. **64**, 227411 (2021), arXiv: 2006.10988.
11 V. I. Anisimov, D. Bukhvalov, and T. M. Rice, Phys. Rev. B **59**, 7901 (1999).
12 P. Worm, L. Si, M. Kitatani, R. Arita, J. M. Tomczak, and K. Held, Phys. Rev. Mater. **6**, L091801 (2022).
13 G. A. Pan, D. Ferenc Segedin, H. LaBollita, Q. Song, E. M. Nica, B. H. Goodge, A. T. Pierce, S. Doyle, S. Novakov, D. Córdova Carrizales, A. T. N'Diaye, P. Shafer, H. Paik, J. T. Heron, J. A. Mason, A. Yacoby, L. F. Kourkoutis, O. Erten, C. M. Brooks, A. S. Botana, and J. A. Mundy, Nat. Mater. **21**, 160 (2022), arXiv: 2109.09726.
14 X. Ding, S. Shen, H. Leng, M. Xu, Y. Zhao, J. Zhao, X. Sui, X. Wu, H. Xiao, X. Zu, B. Huang, H. Luo, P. Yu, and L. Qiao, Sci. China-Phys. Mech. Astron. **65**, 267411 (2022), arXiv: 2201.13032.

15 X. Zhou, X. Zhang, J. Yi, P. Qin, Z. Feng, P. Jiang, Z. Zhong, H. Yan, X. Wang, H. Chen, H. Wu, X. Zhang, Z. Meng, X. Yu, M. B. H. Breese, J. Cao, J. Wang, C. Jiang, and Z. Liu, Adv. Mater. **34**, 2106117 (2022).
16 N. N. Wang, M. W. Yang, Z. Yang, K. Y. Chen, H. Zhang, Q. H. Zhang, Z. H. Zhu, Y. Uwatoko, L. Gu, X. L. Dong, J. P. Sun, K. J. Jin, and J. G. Cheng, Nat. Commun. **13**, 4367 (2022), arXiv: 2109.12811.
17 C. He, X. Ming, Q. Li, X. Zhu, J. Si, and H. H. Wen, J. Phys.-Condens. Matter **33**, 265701 (2021), arXiv: 2010.11777.
18 Q. Li, C. He, J. Si, X. Zhu, Y. Zhang, and H. H. Wen, Commun. Mater. **1**, 16 (2020), arXiv: 1911.02420.
19 M. Huo, Z. Liu, H. Sun, L. Li, H. Lui, C. Huang, F. Liang, B. Shen, and M. Wang, Chin. Phys. B **31**, 107401 (2022).
20 J. Zhang, H. Zheng, Y. Ren, and J. F. Mitchell, Cryst. Growth Des. **17**, 2730 (2017).
21 J. Zhang, H. Zheng, Y. S. Chen, Y. Ren, M. Yonemura, A. Huq, and J. F. Mitchell, Phys. Rev. Mater. **4**, 083402 (2020), arXiv: 1904.10048.
22 H. Guo, Z. W. Li, L. Zhao, Z. Hu, C. F. Chang, C. Y. Kuo, W. Schmidt, A. Piovano, T. W. Pi, O. Sobolev, D. I. Khomskii, L. H. Tjeng, and A. C. Komarek, Nat. Commun. **9**, 43 (2018), arXiv: 1705.02589.
23 J. Zhang, D. Phelan, A. S. Botana, Y. S. Chen, H. Zheng, M. Krogstad, S. G. Wang, Y. Qiu, J. A. Rodriguez-Rivera, R. Osborn, S. Rosenkranz, M. R. Norman, and J. F. Mitchell, Nat. Commun. **11**, 6003 (2020), arXiv: 2004.07897.
24 J. L. García-Muñoz, J. Rodríguez-Carvajal, P. Lacorre, and J. B. Torrance, Phys. Rev. B **46**, 4414 (1992).
25 J. Zhang, Y. S. Chen, D. Phelan, H. Zheng, M. R. Norman, and J. F. Mitchell, Proc. Natl. Acad. Sci. USA **113**, 8945 (2016), arXiv: 1601.03711.
26 J. Zhang, D. M. Pajerowski, A. S. Botana, H. Zheng, L. Harriger, J. Rodriguez-Rivera, J. P. C. Ruff, N. J. Schreiber, B. Wang, Y. S. Chen, W. C. Chen, M. R. Norman, S. Rosenkranz, J. F. Mitchell, and D. Phelan, Phys. Rev. Lett. **122**, 247201 (2019), arXiv: 1903.03246.
27 K. Sreedhar, M. McElfresh, D. Perry, D. Kim, P. Metcalf, and J. M. Honig, J. Solid State Chem. **110**, 208 (1994).
28 Z. Zhang, M. Greenblatt, and J. B. Goodenough, J. Solid State Chem. **108**, 402 (1994).
29 S. Taniguchi, T. Nishikawa, Y. Yasui, Y. Kobayashi, J. Takeda, S. Shamoto, and M. Sato, J. Phys. Soc. Jpn. **64**, 1644 (1995).
30 Y. Kobayashi, S. Taniguchi, M. Kasai, M. Sato, T. Nishioka, and M. Kontani, J. Phys. Soc. Jpn. **65**, 3978 (1996).
31 C. D. Ling, D. N. Argyriou, G. Wu, and J. J. Neumeier, J. Solid State Chem. **152**, 517 (1999).
32 Z. Zhang, and M. Greenblatt, J. Solid State Chem. **117**, 236 (1995).
33 X. Fan, and H. H. Wen, J. Phys.-Condens. Matter **33**, 075503 (2020).
34 G. Wu, J. J. Neumeier, and M. F. Hundley, Phys. Rev. B **63**, 245120 (2001).
35 D. K. Seo, W. Liang, M. H. Whangbo, Z. Zhang, and M. Greenblatt, Inorg. Chem. **35**, 6396 (1996).
36 A. S. Botana, V. Pardo, W. E. Pickett, and M. R. Norman, Phys. Rev. B **94**, 081105 (2016), arXiv: 1604.06326.
37 V. V. Poltavets, M. Greenblatt, G. H. Fecher, and C. Felser, Phys. Rev. Lett. **102**, 046405 (2009).
38 N. apRoberts-Warren, J. Crocker, A. P. Dioguardi, K. R. Shirer, V. V. Poltavets, M. Greenblatt, P. Klavins, and N. J. Curro, Phys. Rev. B **88**, 075124 (2013), arXiv: 1308.1322.
39 W. Cai, H. Sun, W. Xia, C. Wu, Y. Liu, H. Liu, Y. Gong, D. X. Yao, Y. Guo, and M. Wang, Phys. Rev. B **102**, 144525 (2020), arXiv: 1912.05166.
40 H. Sun, C. Chen, Y. Hou, W. Wang, Y. Gong, M. Huo, L. Li, J. Yu, W. Cai, N. Liu, R. Wu, D. X. Yao, and M. Wang, Sci. China-Phys. Mech. Astron. **64**, 118211 (2021), arXiv: 2104.09412.
41 L. Li, X. Hu, Z. Liu, J. Yu, B. Cheng, S. Deng, L. He, K. Cao, D. X. Yao, and M. Wang, Sci. China-Phys. Mech. Astron. **64**, 287412 (2021), arXiv: 2105.09556.
42 V. V. Poltavets, K. A. Lokshin, S. Dikmen, M. Croft, T. Egami, and M. Greenblatt, J. Am. Chem. Soc. **128**, 9050 (2006).
43 L. Qiao, and X. Bi, Europhys. Lett. **93**, 57002 (2011).
44 Y. Liu, P. Liu, W. Qin, X. Wu, and G. Yang, Electrochim. Acta **297**, 623 (2019).
45 H. Chen, Z. Wu, Y. Zhong, T. Chen, X. Liu, J. Qu, W. Xiang, J. Li, X. Chen, X. Guo, and B. Zhong, Electrochim. Acta **308**, 64 (2019).
46 F. Rivadulla, J. S. Zhou, and J. B. Goodenough, Phys. Rev. B **67**, 165110 (2003), arXiv: cond-mat/0302426.
47 C. Liu, V. F. C. Humbert, T. M. Bretz-Sullivan, G. Wang, D. Hong, F. Wrobel, J. Zhang, J. D. Hoffman, J. E. Pearson, J. S. Jiang, C. Chang, A. Suslov, N. Mason, M. R. Norman, and A. Bhattacharya, Nat. Commun. **11**, 1402 (2020), arXiv: 2002.04159.
48 L. Li, N. Narayanan, S. Jin, J. Yu, Z. Liu, H. Sun, C. W. Wang, V. K. Peterson, Y. Liu, S. Danilkin, D. X. Yao, D. Yu, and M. Wang, Phys. Rev. B **102**, 094413 (2020), arXiv: 2006.03356.
49 L. Ortega-San Martin, J. P. Chapman, L. Lezama, J. Sánchez Marcos, J. Rodríguez-Fernández, M. I. Arriortua, and T. Rojo, Eur. J. Inorg. Chem. **2006(7)**, 1362 (2006).
50 K. P. Rajeev, G. V. Shivashankar, and A. K. Raychaudhuri, Solid State Commun. **79**, 591 (1991).
51 C. H. Chen, S. W. Cheong, and A. S. Cooper, Phys. Rev. Lett. **71**, 2461 (1993).
52 S. H. Lee, and S. W. Cheong, Phys. Rev. Lett. **79**, 2514 (1997), arXiv: cond-mat/9706110.
53 R. Zhong, B. L. Winn, G. Gu, D. Reznik, and J. M. Tranquada, Phys. Rev. Lett. **118**, 177601 (2017), arXiv: 1608.04799.